Lawrence Berkeley National Laboratory
Recent Work

Title
CYCLOTRON SHIELDING

Permalink
https://escholarship.org/uc/item/63g046gd

Author
Wallace, Roger.

Publication Date
1965-08-11

eScholarship.org Powered by the California Digital Library
University of California

UCRL-11315

c.2

University of California

Ernest O. Lawrence Radiation Laboratory

CYCLOTRON SHIELDING

TWO-WEEK LOAN COPY

This is a Library Circulating Copy which may be borrowed for two weeks. For a personal retention copy, call Tech. Info. Division, Ext. 5545

Berkeley, California

UCRL-11315 c.2

DISCLAIMER

This document was prepared as an account of work sponsored by the United States Government. While this document is believed to contain correct information, neither the United States Government nor any agency thereof, nor the Regents of the University of California, nor any of their employees, makes any warranty, express or implied, or assumes any legal responsibility for the accuracy, completeness, or usefulness of any information, apparatus, product, or process disclosed, or represents that its use would not infringe privately owned rights. Reference herein to any specific commercial product, process, or service by its trade name, trademark, manufacturer, or otherwise, does not necessarily constitute or imply its endorsement, recommendation, or favoring by the United States Government or any agency thereof, or the Regents of the University of California. The views and opinions of authors expressed herein do not necessarily state or reflect those of the United States Government or any agency thereof or the Regents of the University of California.

Submitted to Engineering Compendium
on Radiation Shielding

UCRL-11315

UNIVERSITY OF CALIFORNIA

Lawrence Radiation Laboratory
Berkeley, California

AEC Contract No. W-7405-eng-48

CYCLOTRON SHIELDING

Roger Wallace

August 11, 1965

CYCLOTRON SHIELDING*

Roger Wallace

Lawrence Radiation Laboratory
University of California
Berkeley, California

August 11, 1965

ABSTRACT

The shielding required for a cyclotron can be estimated by computing the emission spectra of the neutrons produced, and using these spectra to estimate the necessary thickness of shielding to reduce the radiation level at a specified location to a safe level. The prediction of the secondary neutron spectrum produced inside a thick shield is described. The multiplicity of cascade and evaporation secondaries as well as subsequent moderation of the secondary spectrum is described quantitatively. Experimental thick-target neutron yields, as well as Monte Carlo cascade data, are the basis for these estimates.

1. Introduction

The calculation of the required shielding of a several-hundred-MeV cyclotron is approximately the same as for any other accelerator operating in the same energy range. The only substantial difference is probably the higher beam current of the cyclotron. The special techniques used to achieve these higher beam currents do not have any bearing on the shielding or activation problem, and the experience gained in shielding low-current cyclotrons in the same energy range is directly applicable to modern high-current ($\geq 100\,\mu$ amps) cyclotrons. Since a several-hundred-MeV modern cyclotron is fairly large physically, the shielding is quite expensive and is a major item in the budget. Thus, it is not appropriate to use large safety factors for the shielding thickness, as might be done for a small machine. As a result the necessary shielding thickness must be explored in greater detail than has sometimes been done in the past. In some early cyclotrons, the shielding was sometimes treated as an afterthought or an accessory that could be added to a later date, when the initial construction expense of the accelerator itself was a few years in the past. A modern high-current cyclotron cannot be used effectively from its startup without the correct amount of shielding. The neutron-capture induced-activity problem presents an additional problem in subsequent maintenance and modification, which must not be postponed until after construction.

Unfortunately these problems are not of great basic scientific interest, consequently calculations have only recently been made with shielding primarily in mind. Some day very detailed Monte Carlo computations will be available, taking into consideration energy and angular distributions, and various geometrical situations, in a more rigorous manner. Such calculations are well along at the Oak Ridge National Laboratories in connection with the radiation-dose estimate for the project to send a man to the moon.

These calculations are directed toward shielding against solar-flare protons, but the lunar project is in many ways very similar to the cyclotron shielding problem.

In the shielding of a cyclotron in the several-hundred-MeV range the secondary neutrons produced by the main-beam protons in the primary target and in the hardware of the accelerator (and the radioactivity they induce) are the only important source of dose. Sufficient shielding around the accelerator to attenuate the neutrons very completely contains the electromagnetic radiation and the charged particles. The only known exception would be much-higher-energy machines, in which μ mesons may be the controlling factor. Such will not be the case at several hundred MeV.

Method of Calculation

The technique generally used to estimate shielding is that developed by Moyer.[1,2,3] While each proton produces a variety of particles as it undergoes collision in the shield, only the neutrons are of biological significance. For protons striking an extended thick target, the total neutron production as a function of energy for carbon, aluminum, copper, and lead is shown in Fig. 1. This total neutron production consists of two parts, "cascade" and "evaporation" neutrons. There are also cascade protons. The particles that are knocked out during the immediate passage of the incident proton by direct interactions between the proton and the individual nucleons in a target nucleus have been extensively treated by Metropolis.[4] The cascade particles, because of momentum conservation, are strongly concentrated in the forward direction relative to the incident-proton direction. Because of their long mean free paths, only those cascade particles having energies above 150 MeV need be considered in shielding. Cascade particles would be rather unimportant as secondaries from protons of less than 100 MeV.

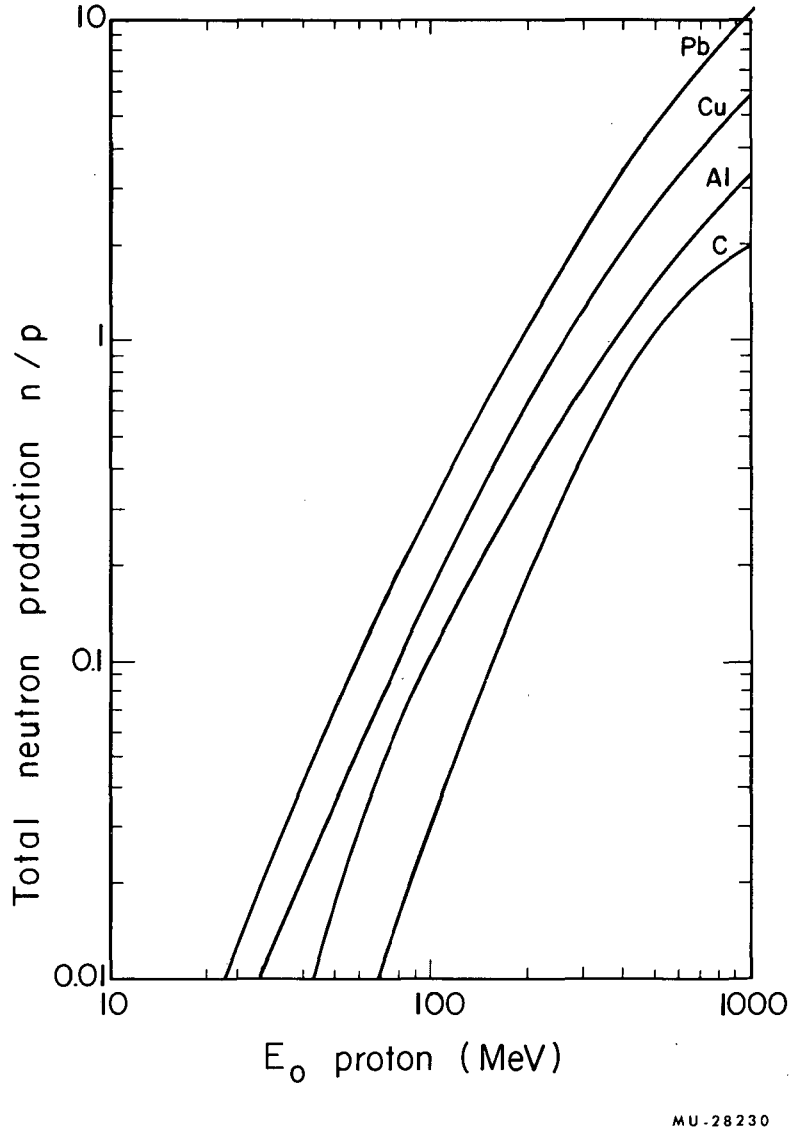

Fig. 1. Measured total neutron yields per proton stopping in a thick target for C, Al, Cu, and Pb. From Moyer (reference 2).

The rest of the secondary particles are produced, after the initial proton passage, by evaporation from the nucleus as a result of the excitation energy left behind in the nucleus. The evaporation process gives off neutrons isotropically. These curves (do include the production from) plural cascade within the target nucleus. The cascade yields of neutrons and protons resulting from either neutron or proton bombardment are shown in Fig. 2.

Neutron Spectra

The resulting secondary-neutron spectrum (which will be seen in Fig. 22) consists of three parts:

(a) the cascade neutrons of more than 20 MeV,

(b) the evaporation-neutron spectrum, peaked in the few-MeV region, and

(c) the resulting thermal spectrum, which arises from the degradation of the energy of the other two neutron sources.

This three-part spectrum is a convenient natural breakdown of this problem, otherwise far too complex for a simple estimate. (Of course, the problem is not too complex for a computer approach.) The cascade neutrons above 150 MeV are the only part of the total spectrum that must initially be considered in estimating the thickness of the shield; because neutrons of lower energy have attenuation lengths substantially shorter than those with energies above 150 MeV. It is only this penetrating high-energy component that determines the shield thickness, as can be seen in Figs. 3 and 4. There is a plateau in the half-value thicknesses of concrete shielding above 150 MeV. The conclusions that one reaches about concrete are also applicable to most other materials (with the exception of hydrogen) on the basis of grams/cm^2. A thick shield made of liquid hydrogen would need special consideration.

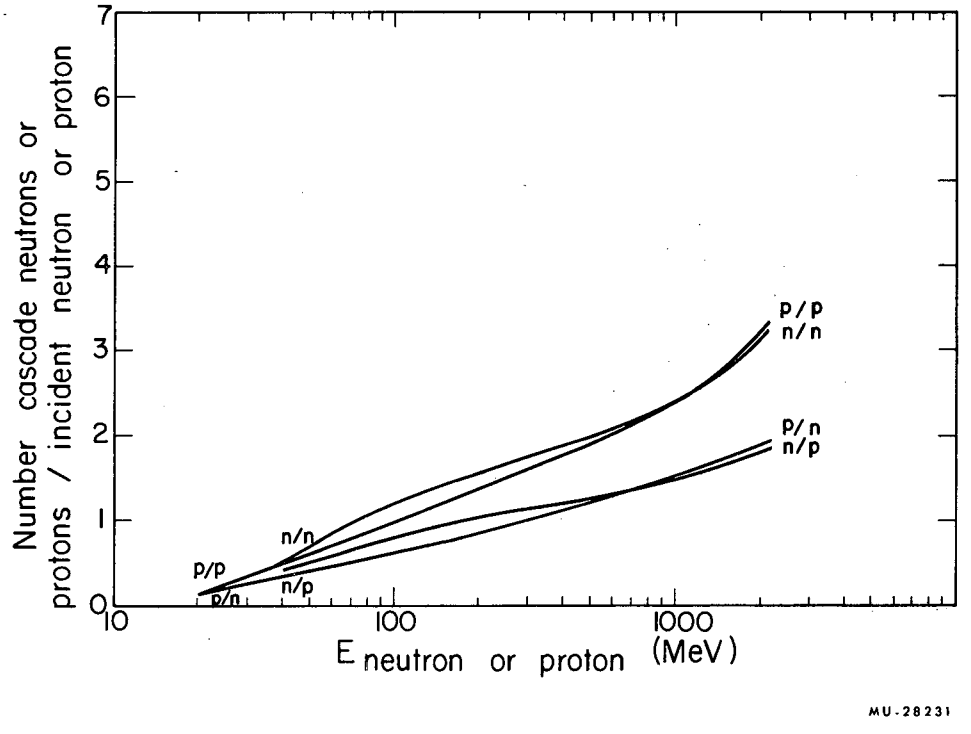

Fig. 2. Estimated cascade neutrons and protons produced by incident neutrons or protons of energy E_n on nuclei near A = 20 per incident particle per inelastic collision. From Metropolis et al. (reference 4).

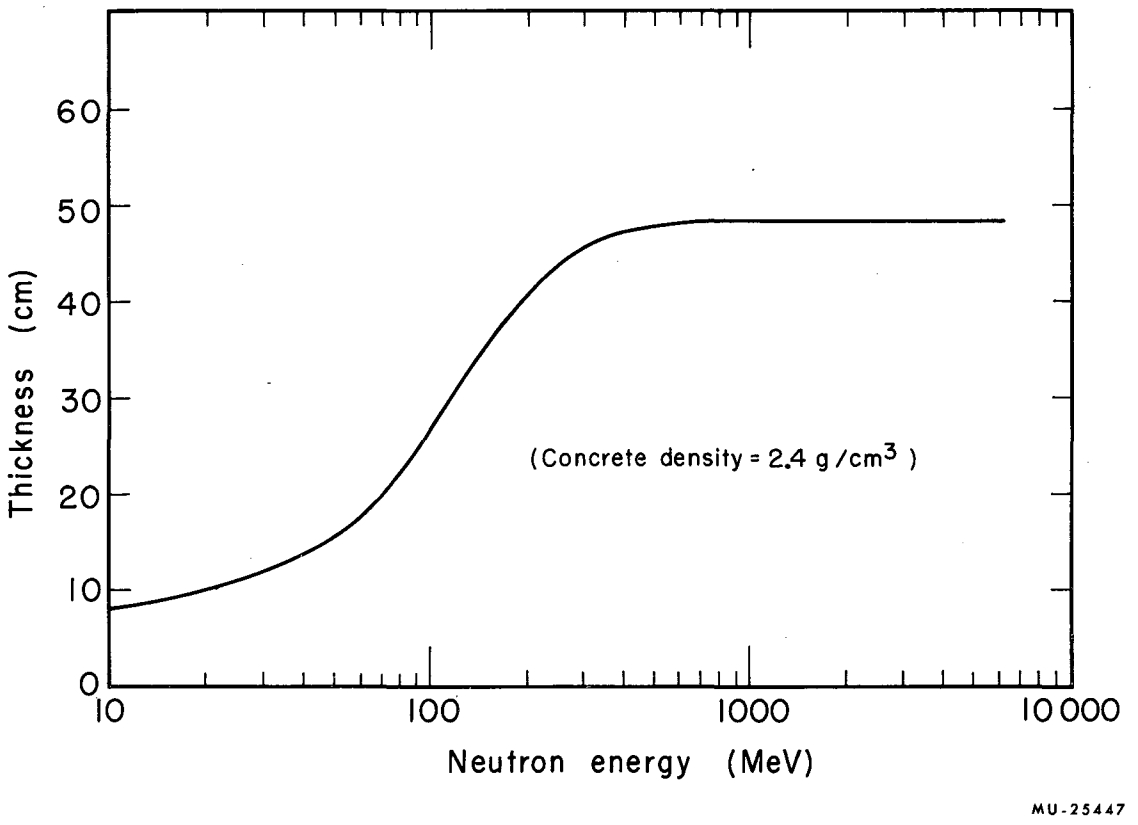

Fig. 3. Half-value thickness for high-energy neutrons in ordinary concrete.

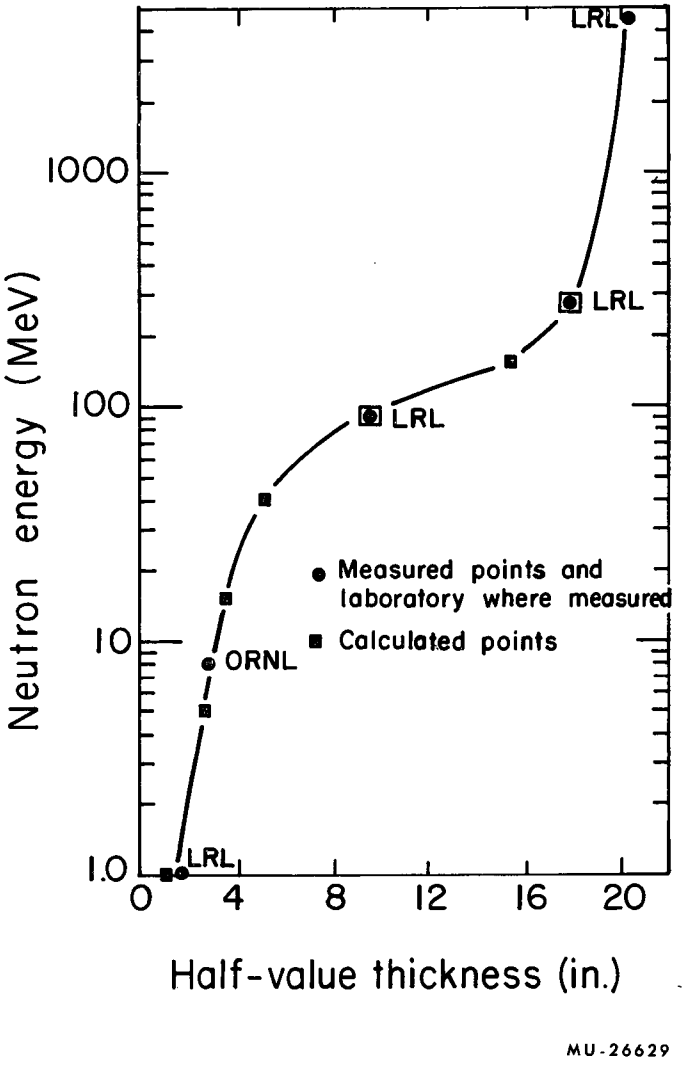

Fig. 4. Attenuation of neutrons in ordinary concrete. At 90 and 270 MeV, measurements were made at the 184-inch 340-MeV cyclotron. At 4.5 GeV the measurement was made at the Bevatron.

There is, of course, a buildup and an establishment of equilibrium in the secondary neutron spectrum in the first few layers of the shield. After equilibrium is established in one or two half-value layers, no further change in the shape of the neutron spectrum occurs with increasing depth in the shield, only an attenuation of the entire spectrum with the same mean attenuation length as that of the highest-energy primaries.

Cascade Particles

The spectra of cascade particles computed by Metropolis[4] are shown in Fig. 5 for 460- and 1840-MeV protons incident on aluminum. These spectra seem to be in good agreement except at the highest energies. These spectra multiplied by the appropriate normalization factors (given in Fig. 6), are shown in the energy region above 1 MeV on Fig. 7 for incident proton energies of 450, 600, and 850 MeV. It is seen that below about 100 MeV the cascade spectra are essentially the same. These spectra have not yet been degraded by passage through hydrogenous material, therefore no thermal peak is present.

The angular distribution of the cascade particles of Metropolis et al.[4] has been augmented by Moyer, using data on the angular distribution of the prongs of nuclear-emulsion stars from the Bevatron and from cosmic rays. A representative angular distribution is shown in Fig. 8. The distribution shown is normalized for 6.2-GeV protons on copper; however, the angular distribution is not sensitive to energy.

The number of cascade neutrons per incident proton per inelastic collision as a function of proton energy is given in Fig. 6 for several target materials. It is seen that for energies above 200 MeV there is a monotonic increase in the number of cascade neutrons with A, whereas for the energy region below 200 MeV the low-A materials actually have a higher neutron

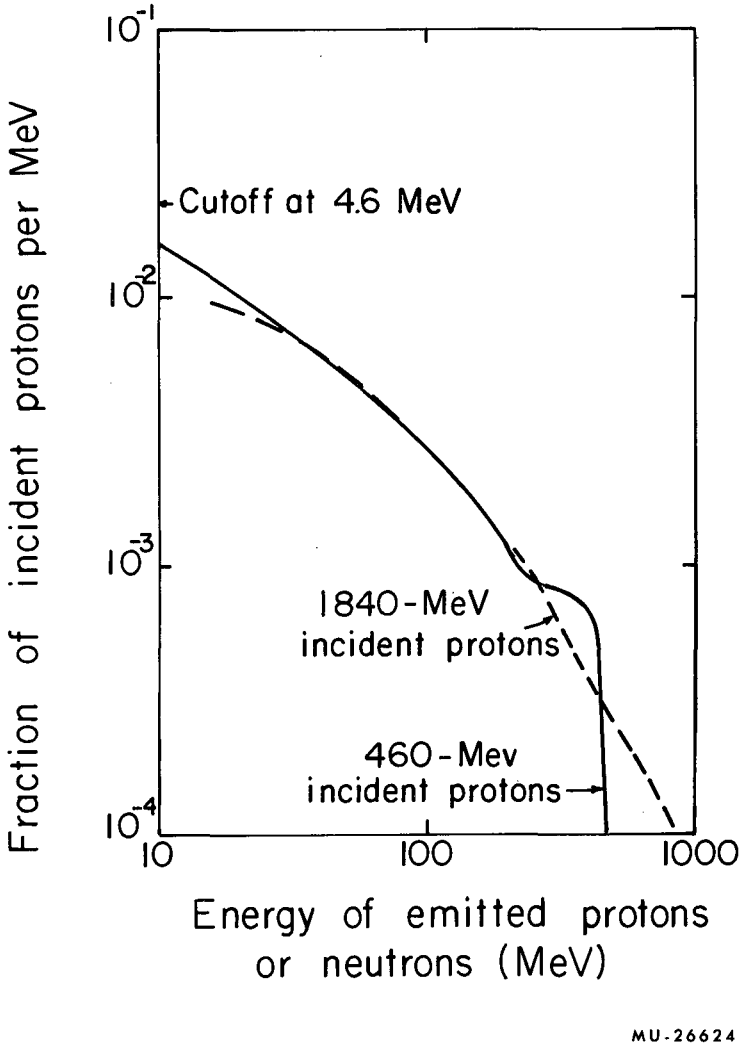

Fig. 5. Energy spectra of cascade nucleons emitted from aluminum. From Metropolis et al. (reference 4).

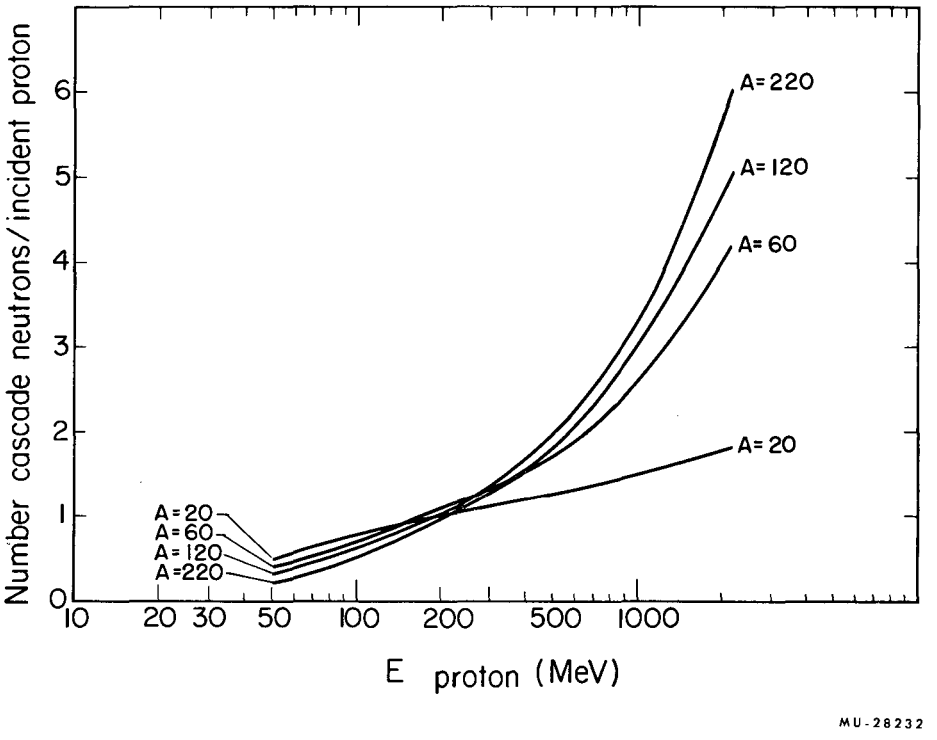

Fig. 6. Number of cascade neutrons per incident proton per inelastic collision as a function of proton energy and target A, from Metropolis et al. (reference 4).

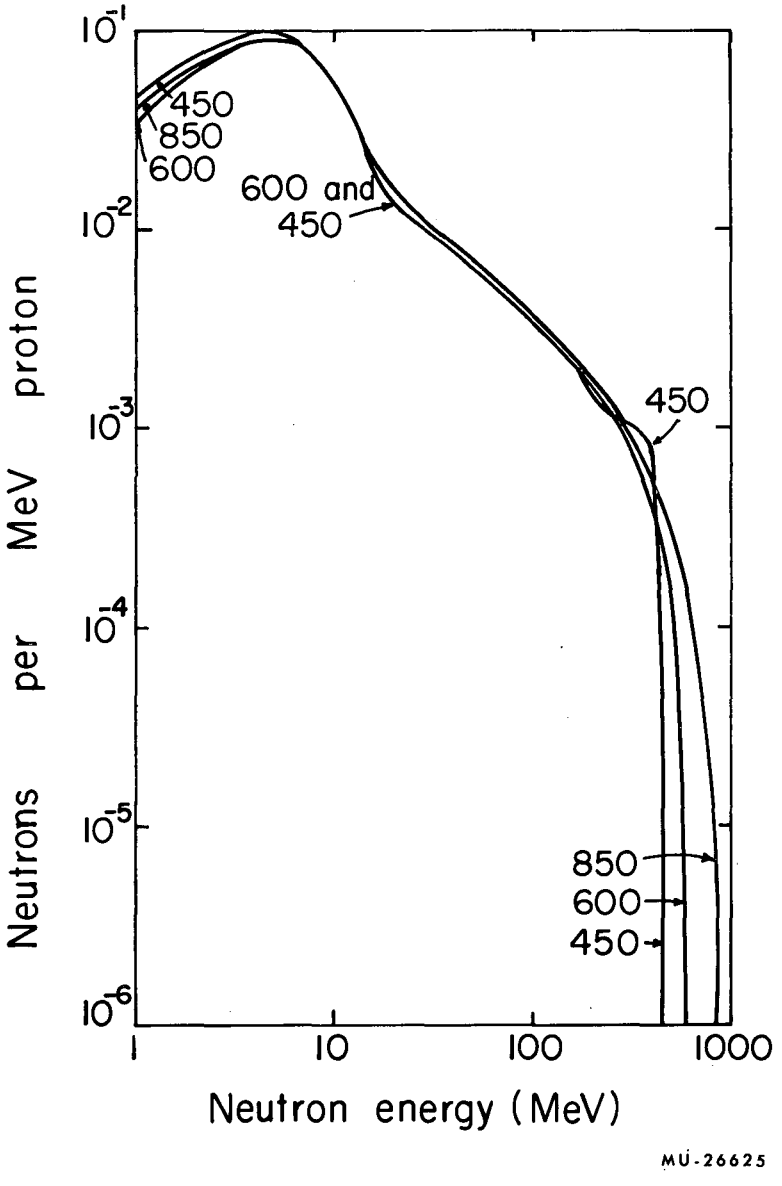

Fig. 7. Cascade and evaporation-neutron emission spectra from 450-, 600-, and 850-MeV protons on aluminum, per incident proton.

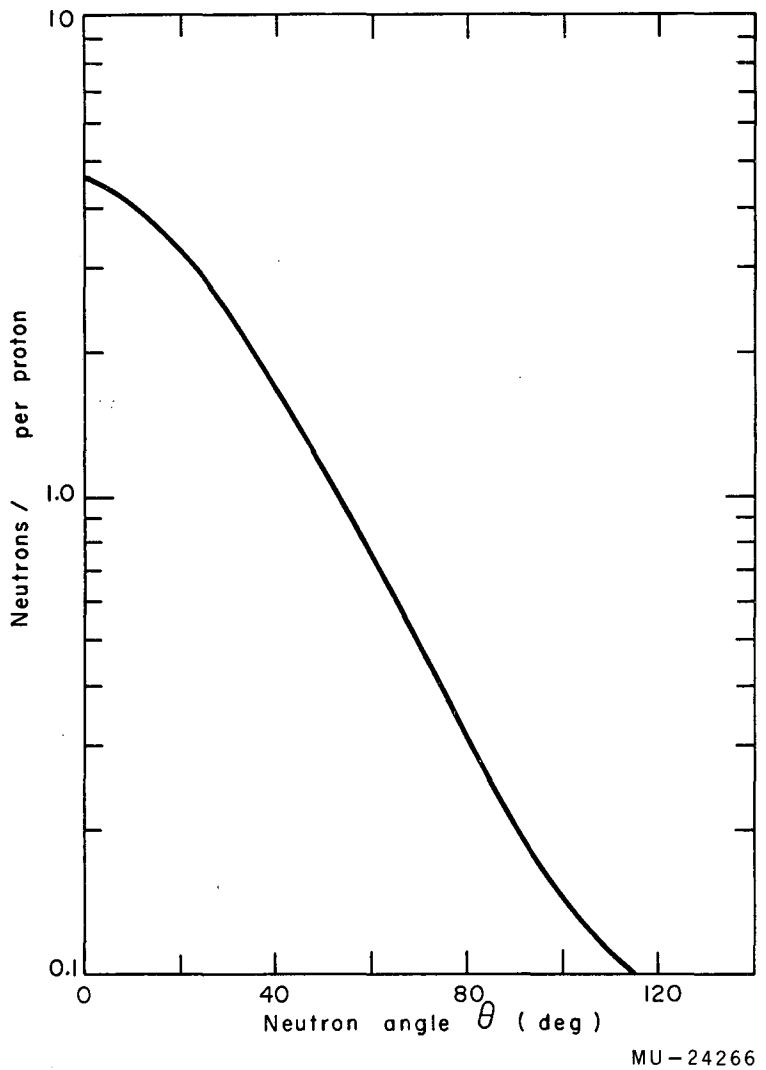

Fig. 8. Angular distribution of neutrons, over 150 MeV in energy, from a single collision in Cu by 6.3-GeV protons (normalized to 8 neutrons/proton), from Metropolis et al. (reference 4).

production than the high-A materials. The inelastic cross sections for C, Al, Cu, and Pb are given in Fig. 9.

The number of cascade protons per incident proton per inelastic collision as a function of proton energy and target A is shown in Fig. 10. These curves bear a resemblance to those for neutron production in Fig. 6, and the same conclusion can be drawn with respect to production in the light elements. It should be noted that in the energy region near 500 MeV the Fig. 10 cascade-proton curves are in the reverse order, with the highest proton production coming from the low A's and the lowest proton production coming from the high A's, in contrast to Fig. 6 cascade neutrons. Above 1000 MeV the low-A curve does cross over the others, but the others still remain in the inverted order. This particular fact is of only minor importance to our present problem, since cascade protons have a very limited range and it is really the cascade neutrons that one must consider.

If the shielding is quite thick, a similar set of curves could be provided, giving neutrons per incident neutron and protons per incident neutron as a function of A and energy. These additional curves would be useful only for some specialized accelerator-shielding situations.

Evaporation Particles

The most important source of neutrons is the evaporation process. Several authors[6-9] have treated the evaporation of nucleons from nuclei that have been excited by very-high-energy neutrons or protons. These evaporation neutrons provide the low-energy end of our spectrum. Nuclear evaporation is somewhat analogous to the evaporation of a liquid on an atomic scale. The resulting particle spectra are obtained by estimating an excitation energy E_1 for the nucleus as a whole. This estimation, due to Moyer,[2] is shown in detail for A from 20 to 220 in Fig. 11. This set of

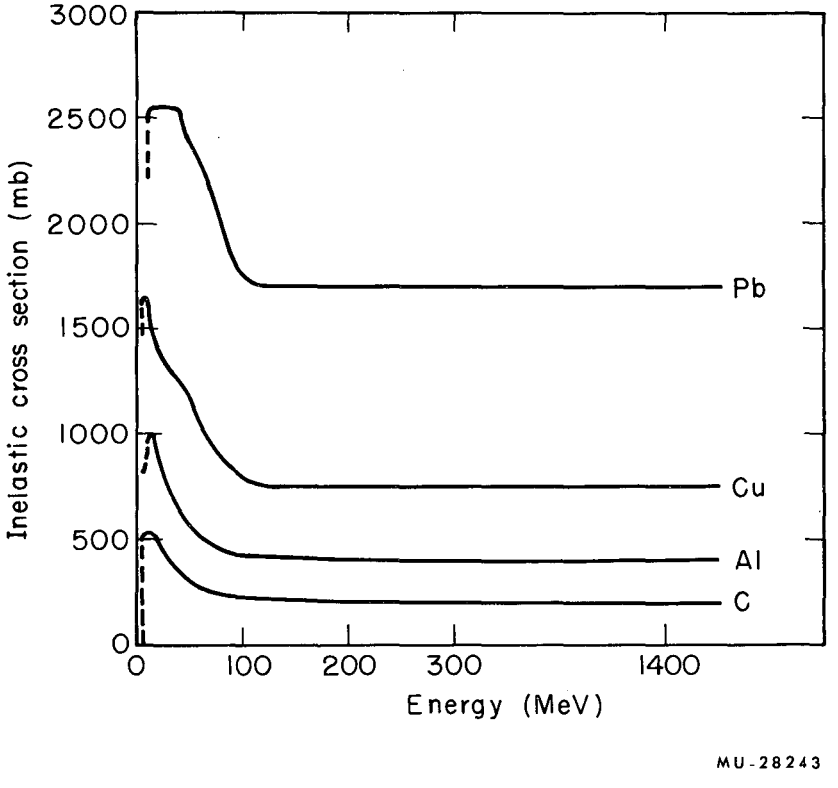

Fig. 9. Neutron or proton inelastic cross sections for C, Al, Cu, and Pb vs incident neutron or proton energy, from Lindenbaum (reference 5).

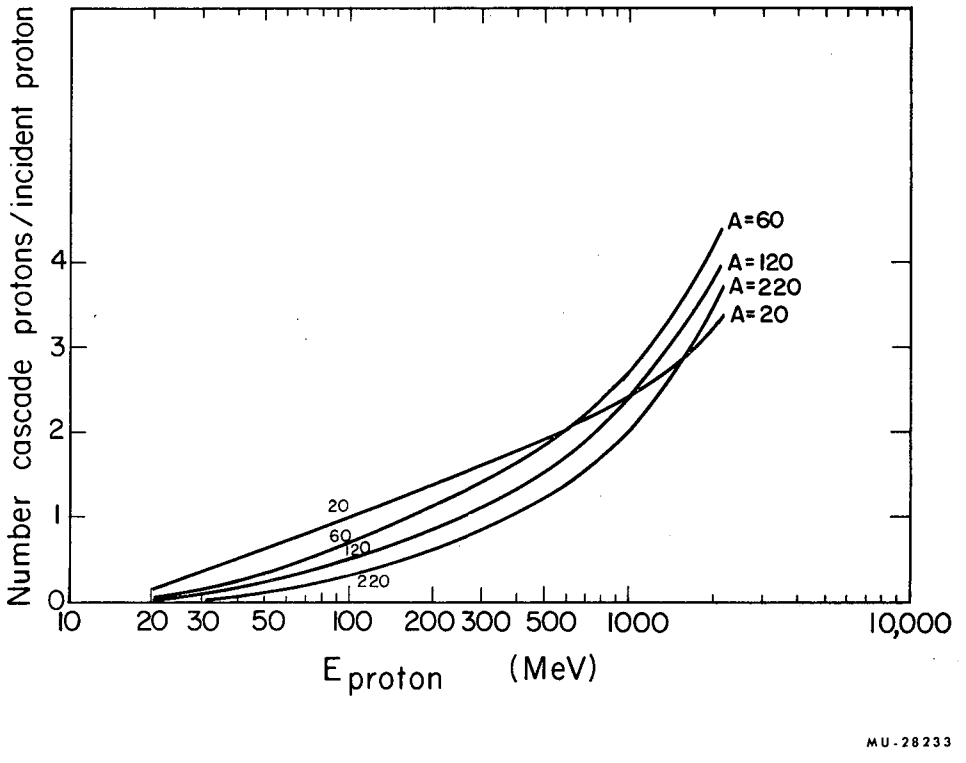

Fig. 10. Number of cascade protons per incident proton per inelastic collision as a function of proton energy and target A, from Metropolis et al. (reference 4).

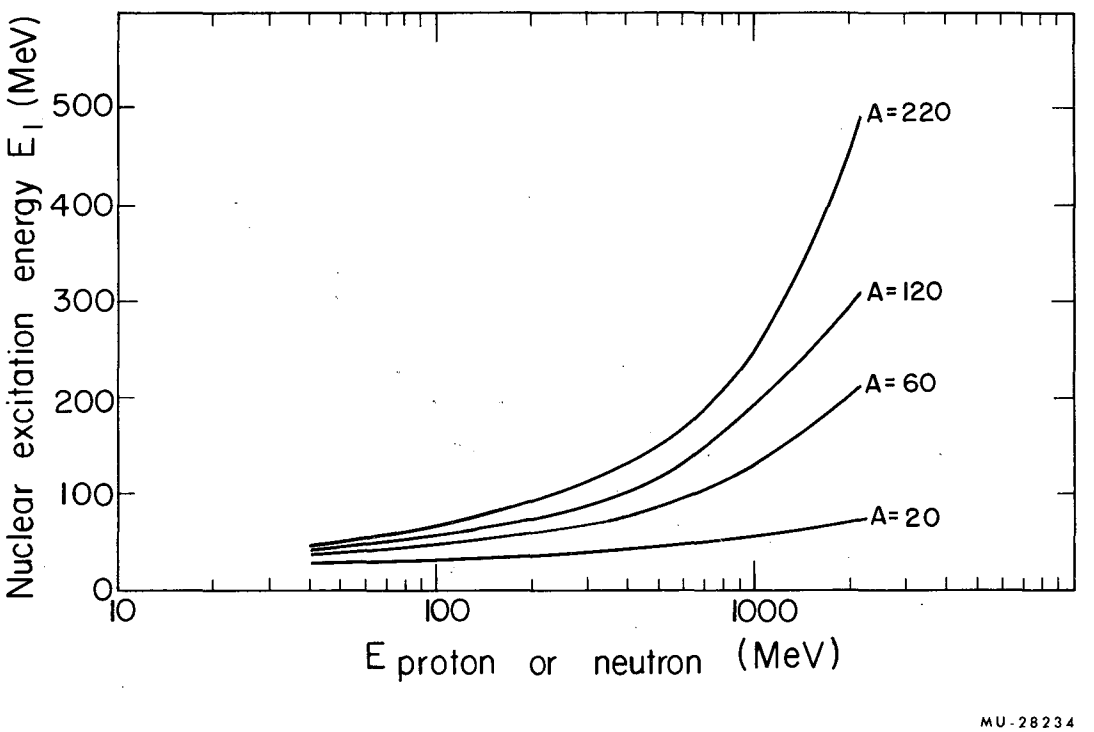

Fig. 11. Average nuclear excitation energy E_1 deposited in nucleus A by an incident neutron or proton of energy E in one inelastic collision.

curves gives the "excitation" energy E_1 left behind in a nucleus by an incident proton or neutron of energy E. This energy is considered as a thermal kinetic-energy source which will eventually lead to evaporation.

The nuclear temperature produced in a nucleus A by the deposition of energy E_1 by an incident neutron or proton is shown in Fig. 12. Note that nuclear temperatures for the light elements have plateaus in the region of several hundred MeV, therefore the change in temperature in this region with increasing incident proton energy is quite small.

The excitation energy is related to the square of an effective nuclear "temperature" τ by an empirical parameter[6] (A/10); thus we have

$$E_1 = (A/10)\tau^2, \tag{1}$$

where E_1 is the nuclear excitation in MeV, and A is the atomic weight of the nucleus. This empirical equation is shown in Fig. 13 for four different values of A. It is seen that the light elements have higher nuclear temperatures than heavy elements at a particular excitation energy. Figures 11, 12, and 13 represent a three-dimensional surface in a space whose coordinates are the total nuclear excitation energy, nuclear temperature, and bombarding-proton energy.

The evaporation spectrum itself is given by

$$N(E)dE = (E/\tau^2)\, e^{-(E/\tau)}\, dE \tag{2}$$

The E in front of the exponential instead of the usual $E^{1/2}$ which appears in the Maxwellian energy distribution is necessary to account for the fact that N(E) is a flux density rather than a numerical density.

To estimate the complete neutron spectrum penetrating the shield, it is now necessary to fit this modified Maxwellian low-energy evaporation end of the spectrum to the Metropolis cascade high-energy tail. This transition fit is made after the area under each individual spectrum has been

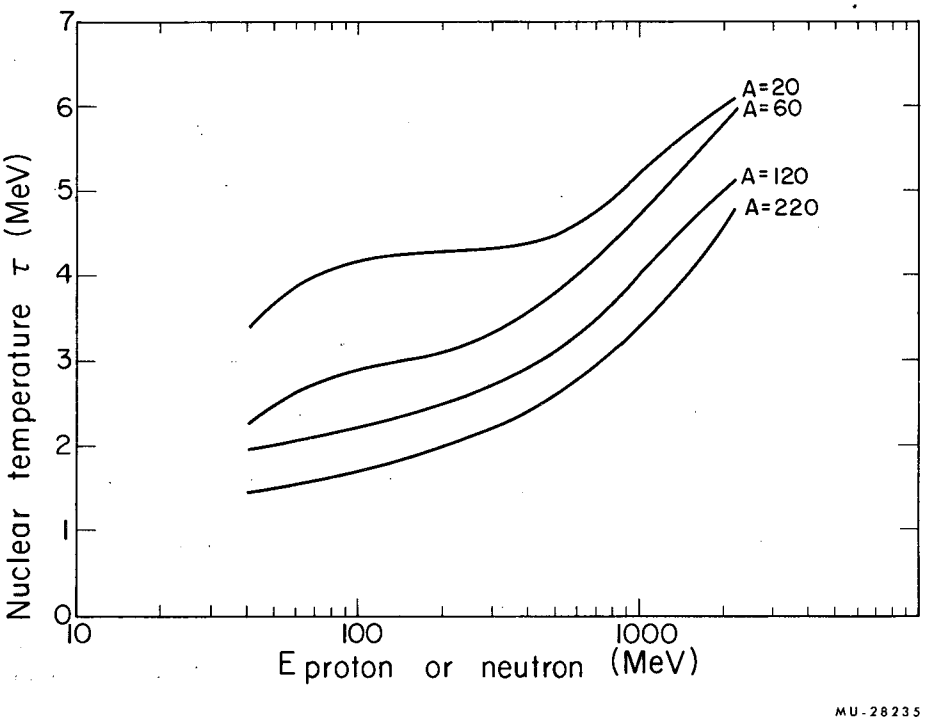

Fig. 12. Estimated residual nuclear temperature produced in nucleus A after excitation by a neutron or proton of energy E in one inelastic collision, from Metropolis et al. (reference 4).

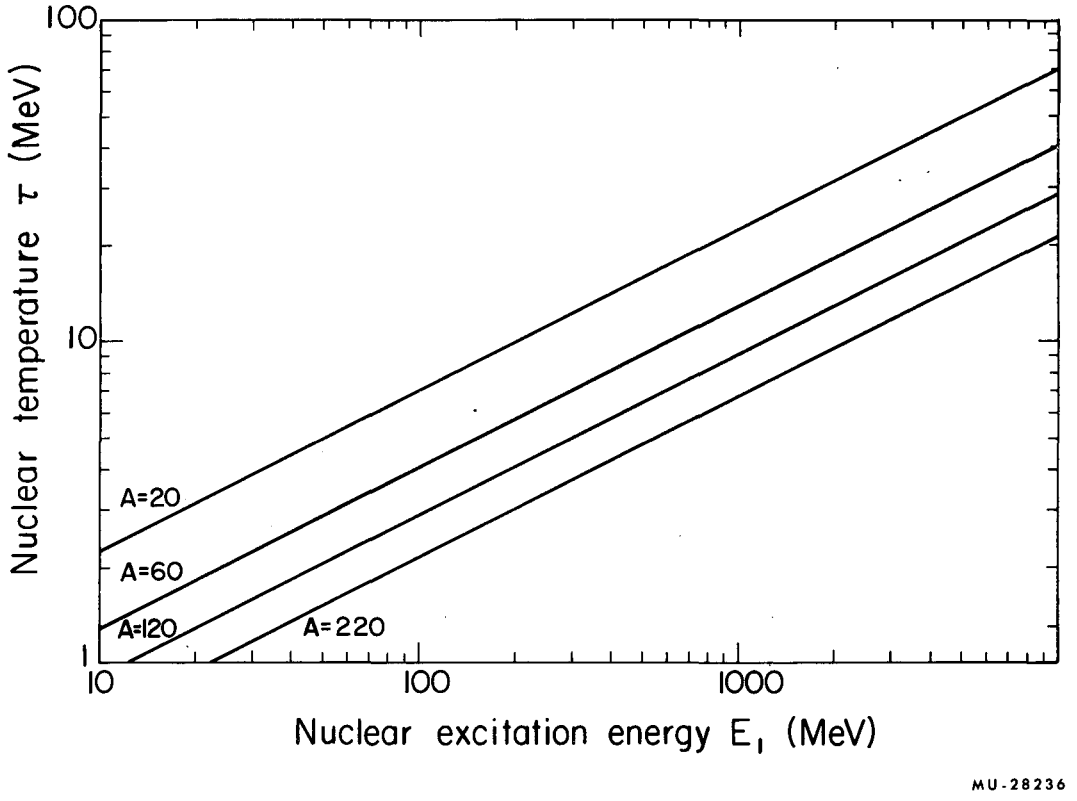

Fig. 13. Nuclear temperature τ vs nuclear excitation energy E_1 for various A's.

normalized to the estimated total production of each spectrum's particular component (as given in Table I for aluminum or shown for other A's and E's in Figs. 1, 6, and 14. Note that in Table I it is appropriate for the sum of "cascade" and "evaporation" neutrons to not equal the "total" neutrons. The "total" production is per incident particle on a thick target. The "cascade" and "evaporation" production are per inelastic collision at the quoted energy. The sum of these two productions can be either less than or greater than the "total," depending on the ratio of proton removal by inelastic collision to proton energy loss by electromagnetic dE/dx. The total neutron production per inelastic collision, and the ratio of the evaporation to the cascade process, as functions of both energy and A, are given in detail in Figs. 15 and 16. The electromagnetic energy loss changes with proton energy, while the inelastic cross sections are quite constant with energy above 100 MeV, as seen in Fig. 9. It is seen that for the lightweight elements the number of evaporation neutrons is quite constant at about one neutron per proton over a wide energy range.

More details of this process are available, such as the suppression of the low-energy particles by the Coulomb barrier, as treated by Dostrovsky[6] and Le Couteur.[7] Singly charged particles such as H, H^2, and H^3, as well as multiply charged particles, such as He^3 and He^4, can also be estimated as given in Figs. 17 through 21. The doubly charged particles have their evaporation spectrum peaks at about twice the energy of the proton spectrum peak for a nucleus of the same excitation. The angular distribution of the particles emitted in connection with nuclear evaporation is of course isotropic. The evaporation particles produced in an internal target have no chance of their own of penetrating the main shield further than the inner one or two mean free paths. Therefore, evaporation particles are mainly of interest with regard to the radioactivity that they may induce in the accelerator

Table I. Secondary cascade and evaporation-particle production, nuclear excitation energy, and temperature for aluminum targets in proton beams of three different energies.

Proton energy (MeV)	Total neutron thick-target yield (n/p)on Al	Number of particles per incident proton on Al per inelastic collision			Residual[a] nuclear excitation E_1 (MeV)	Residual[a] nuclear temperature τ (MeV)	Number of evaporation neutrons per incident or per inelastic collision
		Neutrons[a]	Protons[a]	Total nucleons[a]			
450	1.3	1.30	1.85	3.15	63	4.3	1.30
600	2.1	1.40	2.05	3.45	72	4.5	1.50
850	3.3	1.55	2.25	3.80	88	4.9	1.60

a. See reference 2.

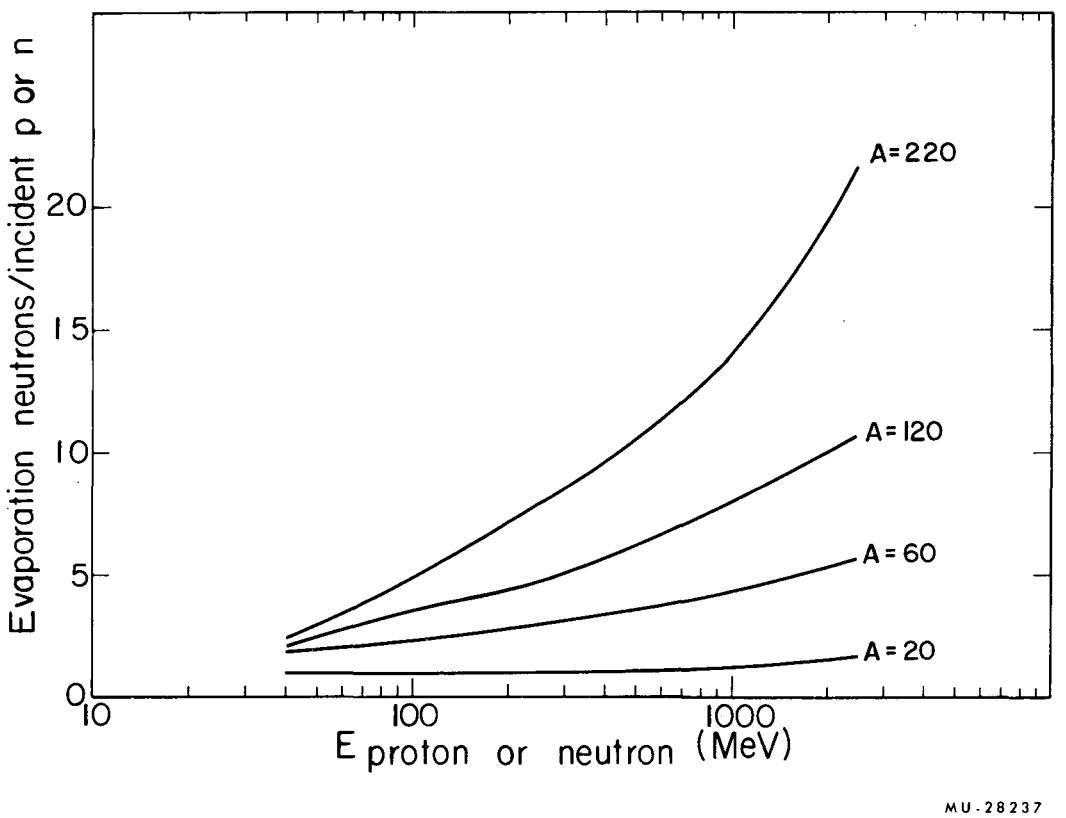

Fig. 14. Estimated number of evaporation neutrons produced per incident neutron or proton of energy E per inelastic collision, from Metropolis et al. (reference 4).

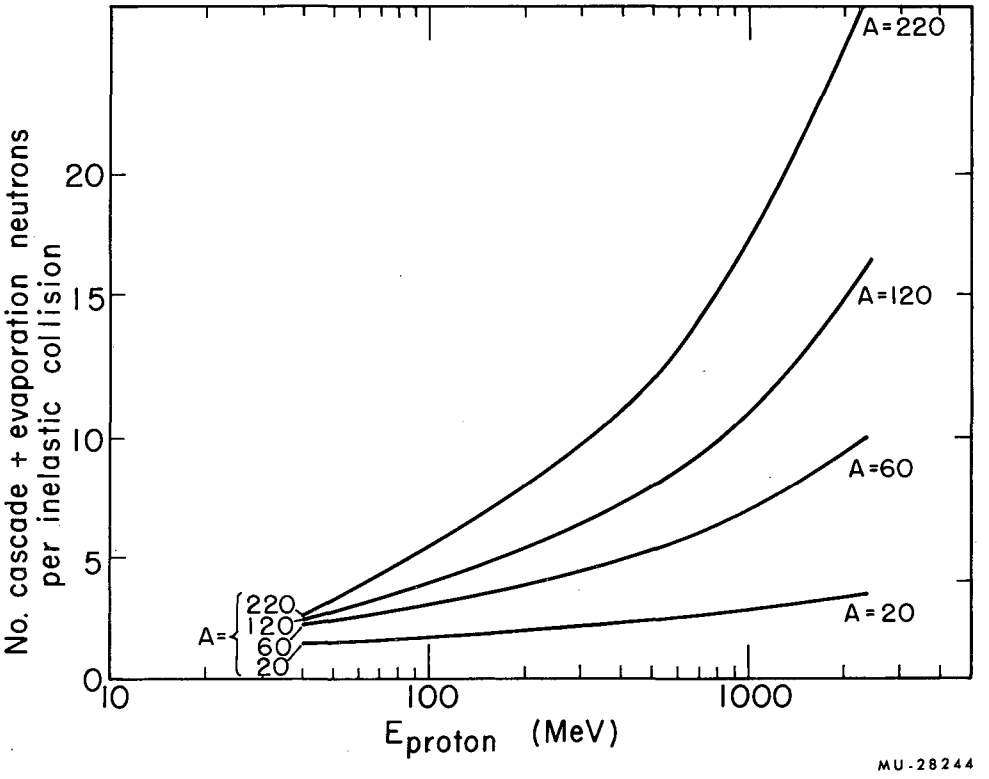

Fig. 15. Total neutron production per inelastic collision = cascade + evaporation as a function of the incident proton energy.

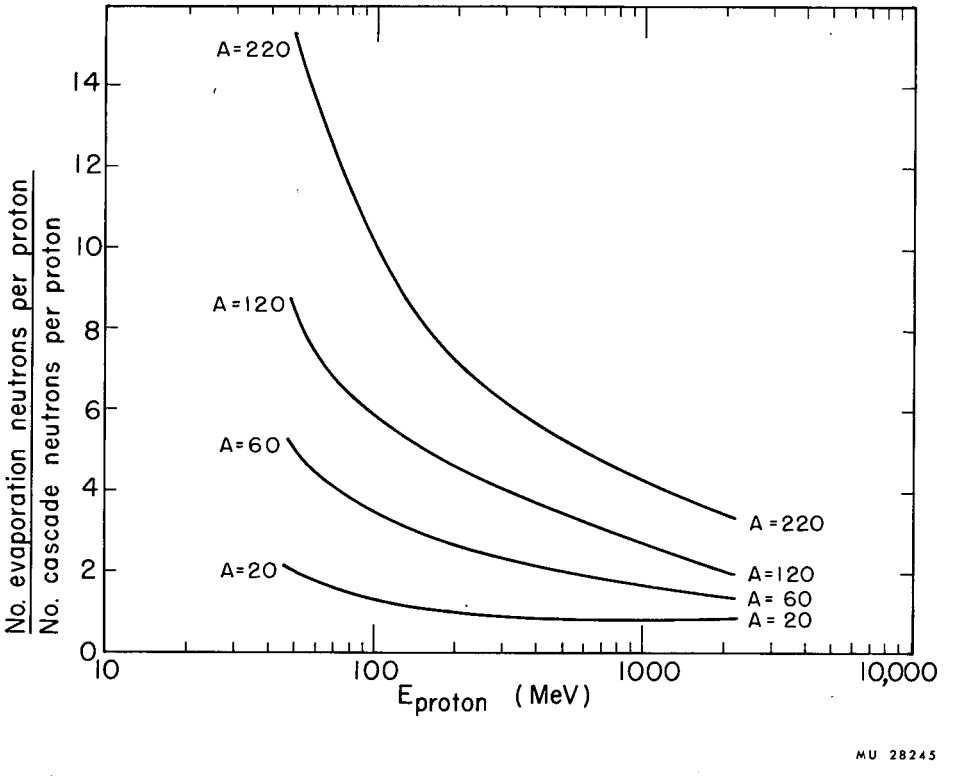

Fig. 16. Ratio of evaporation neutrons to cascade neutrons per inelastic collision as a function of the incident proton energy.

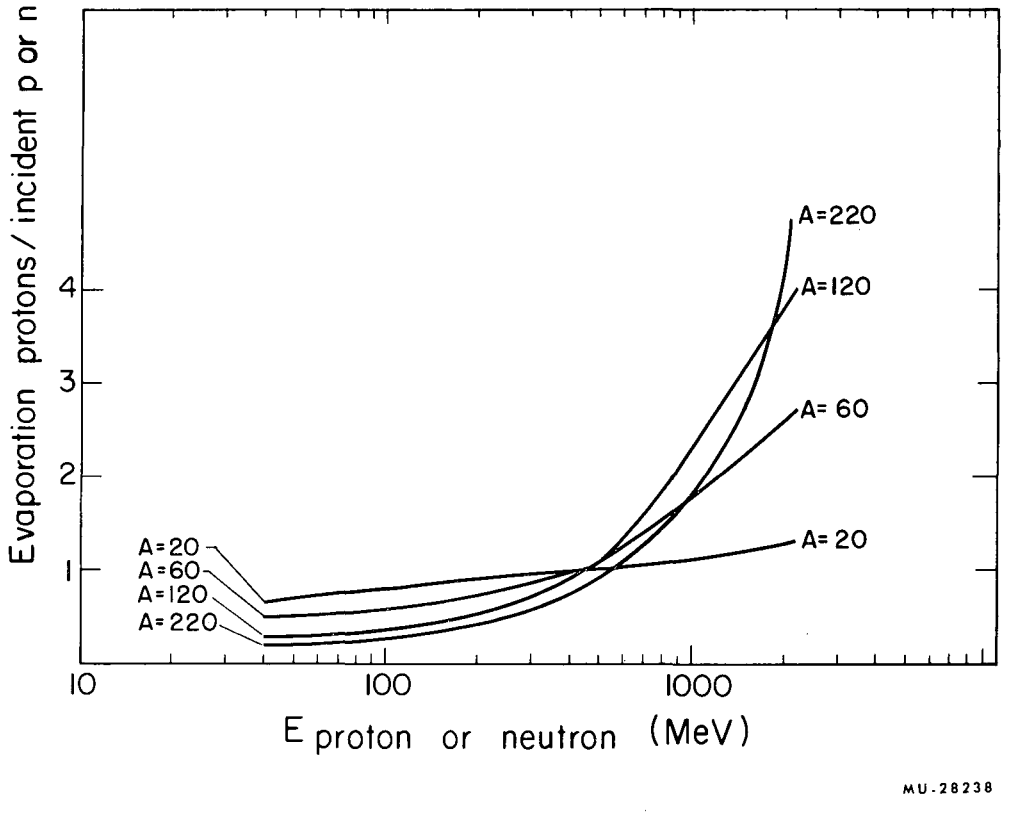

Fig. 17. Average number of evaporation protons per incident proton or neutron on various A's per inelastic collision vs energy of the incident particle, from Metropolis et al. (reference 4).

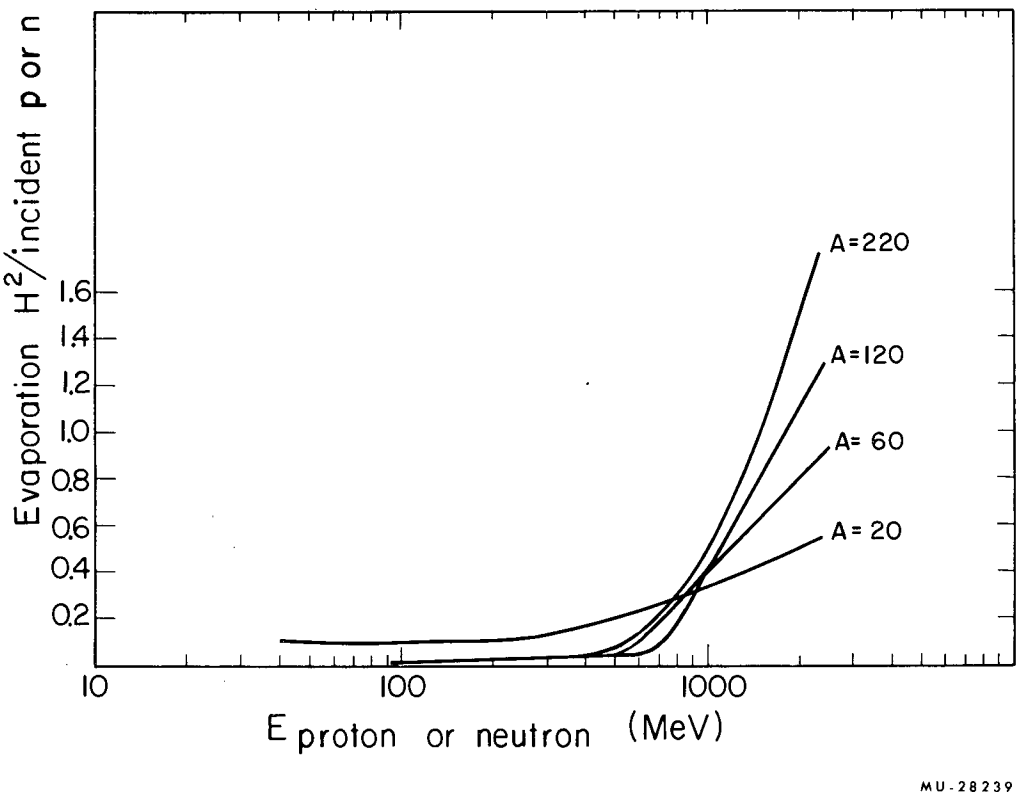

Fig. 18. Average number of evaporation H^2 per incident proton or neutron on various A's per inelastic collision vs energy of the incident particle, from Metropolis et al. (reference 4).

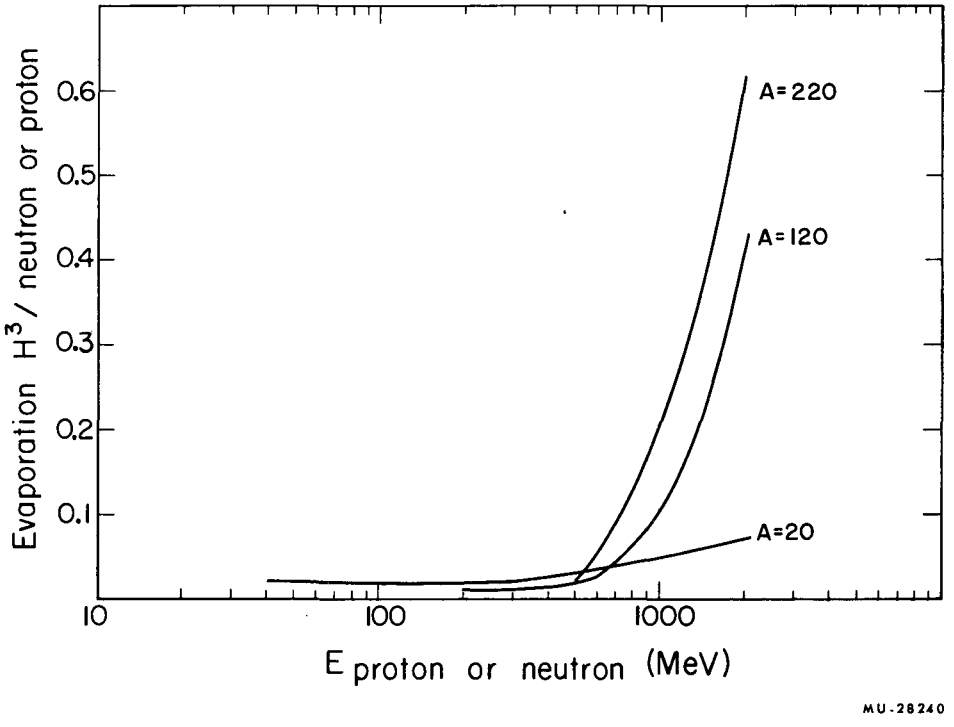

Fig. 19. Average number of evaporation H^3 per incident proton or neutron on various A's per inelastic collision vs energy of the incident particle, from Metropolis et al. (reference 4).

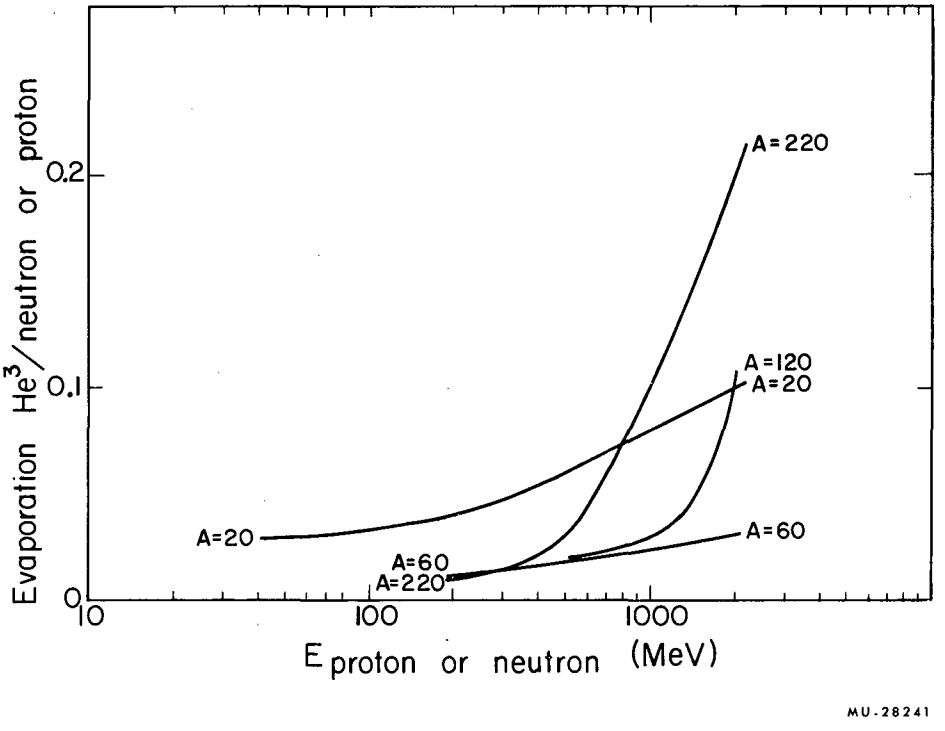

Fig. 20. Average number of evaporation He^3 per incident proton or neutron on various A's per inelastic collision vs energy of the incident particle, from Metropolis et al. (reference 4).

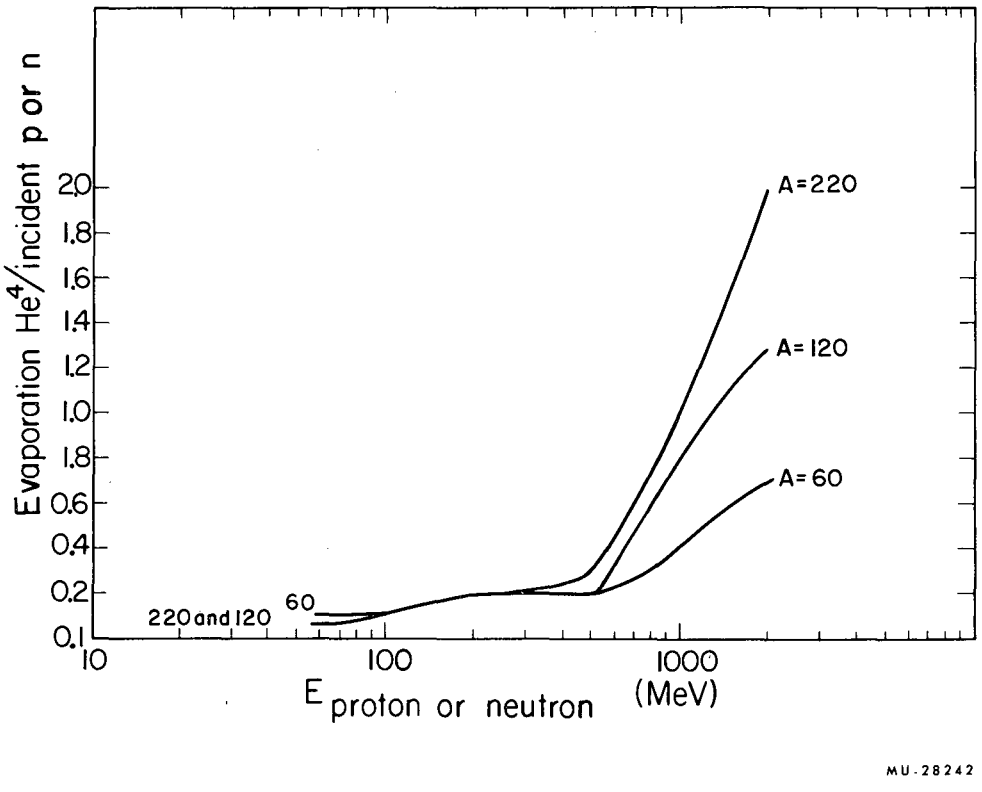

Fig. 21. Average number of evaporation He^4 per incident proton or neutron on various A's per inelastic collision vs energy of the incident particle, from Metropolis et al. (reference 4).

hardware. The evaporation particles are far more important for inducing radioactivity than are the cascade neutrons, since evaporation particles are considerably more numerous and their energy is more favorable for capture. More extensive data are available on evaporation particles.

Epithermal and Thermal Spectra

If one wishes to estimate the spectrum of epithermal neutrons produced by moderation of the cascade and evaporation neutrons and extending below the evaporation peak, the slowing-down spectrum can be approximated by assuming that each emission increment $O(E_1)\Delta E_1$ gives rise to a flux increment with spectrum $1/E-1/E_1$. Thus, by integration, the slowing-down flux has the spectrum

$$\phi(E) = K_1 \int_{E}^{E_{max}} O(E_1) \left(\frac{1}{E} - \frac{1}{E_1}\right) dE_1. \qquad (3)$$

This slowing-down flux spectrum is joined by continuity of slope to the thermal spectrum,

$$\phi_{th} = K_2 E^{1/2} e^{-(E/kT)}, \qquad (4)$$

which is normalized by requiring the integral from zero energy to 1/2 eV to give the value[10]

$$\phi_{th} = 1.25 \frac{Q}{S}, \qquad (5)$$

where Q is the total source strength of fast neutrons and S is the surface area (in cm^2) over which they are thermalized.

Attenuation of the Total Spectrum

Generally the fit between the three parts of the spectra as shown in Fig. 22 is done by eye. Greater accuracy is not appropriate to the degree of approximation we are making. Direct measurements of shield thickness

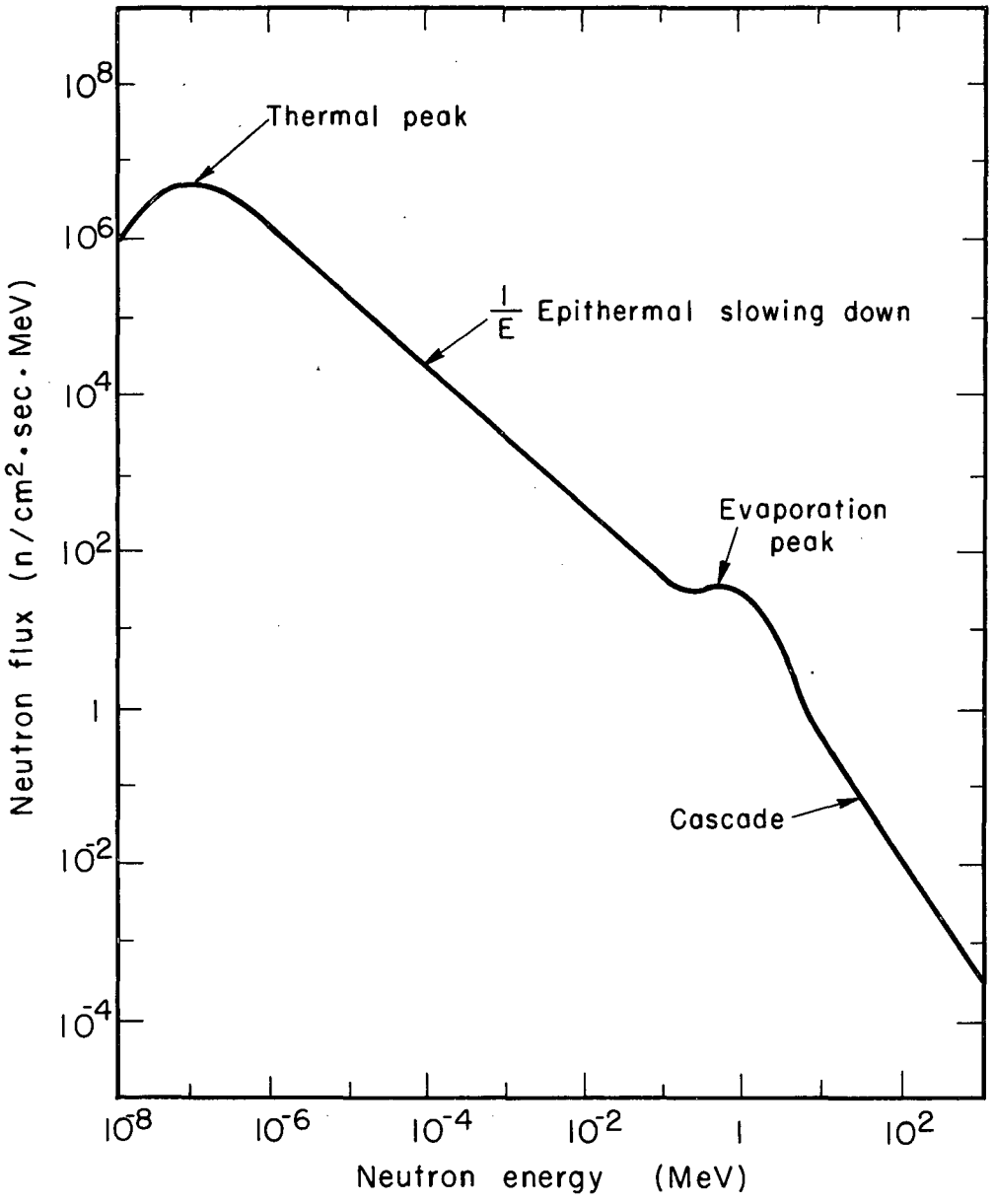

MUB-7392

Fig. 22. The total neutron spectrum consisting of cascade, evaporation, and the resulting slowing-down and thermal-peak neutrons.

required for a given attenuation factor, with use of beams of restricted width, have been made for concrete, water, and a few other materials. Light-weight elements, such as contained in concrete, have shielding values very little different for different A's; this value is mainly proportional to the number of grams of shield per cm^2.

A thick shield provides neutron attenuation by absorbing, degrading, or deviating the neutrons by nuclear collisions. At the high energies characteristic of cascade particles, elastically scattered particles are so strongly peaked in forwardly directed diffraction patterns that essentially no geometric deviation or energy loss occurs. Thus, as the incident neutron energy is increased from values characteristic of the evaporation region to values associated with the cascade region, the value of the effective removal cross section for neutrons by a shield decreases from the value of the total cross section to the value of the inelastic cross section.

This effect is shown in Tables II, III, and IV, from Patterson,[11] as applied to the elements present in ordinary concrete. It is seen that $n\sigma_a(cm^{-1})$ is a figure of merit for the efficiency of each element in the concrete. Table IV emphasizes the importance of the heavier elements as the neutron energy is raised. Several points calculated from these data for concrete, by Patterson, are plotted in Fig. 4 together with several experimental values for energies from 1 MeV to 4.5 GeV. The agreement between the experimental and calculated values is quite good. The same data appear in CGS units in Fig. 3. These data apply only to thick shields and poor geometry.

The measurements of σ_{total} and $\sigma_{reaction}$ for various nuclei as a function of neutron energy up to 5 GeV are given by Coor et al.[12] and Atkinson et al.,[13] and are shown in Lindenbaum.[5] This experimental work shows that the attenuation of neutrons in the high-energy region is essentially constant.

Table II. N(atoms $cm^{-3} \times 10^{22}$) for ordinary concrete.

O	4.73
H	1.73
Si	1.57
Ca	0.26
Al	0.17
Fe	0.053
Na	0.028
K	0.028
Mg	0.013

Table III. Assumed relation between σ_a, the neutron-attenuation cross section, and σ_{tot}, the total neutron cross section.

(MeV)	
1	$\sigma_a = 1.00\ \sigma_{tot}$
5	$\sigma_a = 0.65\ \sigma_{tot}$
14	$\sigma_a = 0.055\ \sigma_{tot}$
≥150	$\sigma_a = 0.50\ \sigma_{tot}$

Table IV. $N\sigma_a(cm^{-1} \times 10^{-2})$ for various elements.

	1 MeV	14 MeV	270 MeV
O	16	4.4	0.89
H	7.8	0.64	0.026
Si	4.7	1.7	0.41
Ca	0.78	0.33	0.10
Al	0.51	0.16	0.05
Fe	0.16	0.045	0.028

Radiation Emerging from the Shield

Now that the spectrum and angular distribution of the neutrons produced in the target and accelerator hardware by the primary protons have been estimated, a secondary calculation can be made of the penetration of the outer shield by these neutrons. This can be done by using similar data for cascade and evaporation particles produced by neutrons (instead of protons as shown in Figs. 2, 11, 12, 14 and 17 through 21) secured from the same sources as given earlier for incident protons. The evaporation data are the same as for incident protons, whereas the cascade values are not. As would be expected, the neutrons are more numerous in neutron-induced cascades than in proton-induced cascades, and protons more numerous for proton-induced cascades. Cascade-produced mesons gradually increase in importance from 500 MeV incident energy on up.

The fluz of particles present outside the accelerator shield consists of (a) directly transmitted primary neutrons of energy >150 MeV (from the spectra shown in Fig. 7), and (b) evaporation fragments produced by the high-energy neutrons that suffer inelastic collisions in the last layers of the shield. The number of cascade neutrons making evaporation neutrons and protons by inelastic collisions within a last layer of the shield wall of thickness x is

$$N = N_0(e^{x/\lambda}-1) ; \qquad (6)$$

where x is measured inward from the outside of the shield, and λ is the mean free path for inelastic collisions of the cascade neutrons. Assume that half the evaporation neutrons emerge. This is an obvious overestimate of the number of evaporation neutrons, but it is to some extent compensated for by the further multiplication of a fraction of the cascade neutrons in secondary collisions, which again increases the number of evaporation

neutrons emerging from the shield. Few of the protons produced in the cascade events in the early part of the shield emerge from the shield, because of range limitations. However, protons that arise from the evaporation processes emerge from the shield.

Considering a final layer of the shield $x = \lambda$, one mean free path thick, and using the spectra shown in Fig. 7 and values of λ shown in Fig. 9 from Lindenbaum,[5] we estimate that in a particular case each cascade neutron produced in the outer shield is accompanied by 0.6 fast neutron and 0.3 proton when it emerges from the shield.

There may also be a small flux of thermal neutrons and gamma rays. The gammas come from thermal neutron capture by the H of the shield (if present) and also from nuclear de-excitations associated with evaporation processes. Typically, the numerical value of the thermal neutron flux is only a few times that of the fast neutrons, so (if we take RBE values into account) the relative dosage from the thermal neutrons is negligible in comparison with the fast neutrons. Ionization-quarter of or less than that arising from fast neutrons.

Acknowledgments.

The author wishes to thank Prof. B. J. Moyer and Mr. H. Wade Patterson for their help in this work.

FOOTNOTES AND REFERENCES

*Work done under auspices of the U. S. Atomic Energy Commission.

1. B. J. Moyer, Method of Calculation of the Shielding Enclosure for the Berkeley Bevatron, in First International Symposium on Protection Near Large Accelerators, Saclay, January 1962.

2. B. J. Moyer (Lawrence Radiation Laboratory), Data Related to Nuclear Star Production by High-Energy Protons, (private communication) June 20, 1961.

3. B. J. Moyer (Lawrence Radiation Laboratory), Shielding and Radiation Calculations for USNRDL Cyclotron, (private communication) October 11, 1960.

4. N. Metropolis, R. Bivins, M. Storm, A. Turkevich, J. M. Miller, and G. Friedlander, Phys. Rev. 110 (1958) 185; and 110 (1958) 204.

5. S. J. Lindenbaum, Shielding of High-Energy Accelerators, in Ann. Rev. Nuclear Sci. 11(1961) 213.

6. I. Dostrovsky, P. Robinowitz, and R. Bivins, Phys. Rev. 111 (1958) 1659.

7. K. J. Le Couteur, Proc. Phys. Soc. (London) A63 (1950) 259.

8. Y. Fujimoto and Y. Yamaguchi, Prog. Theoret. Phys. (Kyoto), 4 468; 5 76; and 5 787 (all in 1950).

9. R. W. Deutsch, Phys. Rev. 97 (1955) 1110-23.

10. H. W. Patterson and R. Wallace, A Method of Calibrating Slow-Neutron Detectors, Lawrence Radiation Laboratory Report UCRL-8359, July 1958 (unpublished).

11. H. Wade Patterson, The Effect of Shielding on Radiation Produced by the 730-MeV Synchrocyclotron and the 6.3-GeV Proton Synchrotron at the Lawrence Radiation Laboratory (UCRL-10061, Jan. 1962); in First International Symposium on Protection Near Large Accelerators, Saclay, Jan. 1962.

12. T. Coor, D. A. Hill, W. F. Hornyak, L. W. Smith, and G. Snow, Phys. Rev. 98 (1955) 1369.

13. J. H. Atkinson, W. N. Hess, V. Perez-Mendez, and R. Wallace, Phys. Rev. 98 (1955) 1369.

This report was prepared as an account of Government sponsored work. Neither the United States, nor the Commission, nor any person acting on behalf of the Commission:

A. Makes any warranty or representation, expressed or implied, with respect to the accuracy, completeness, or usefulness of the information contained in this report, or that the use of any information, apparatus, method, or process disclosed in this report may not infringe privately owned rights; or

B. Assumes any liabilities with respect to the use of, or for damages resulting from the use of any information, apparatus, method, or process disclosed in this report.

As used in the above, "person acting on behalf of the Commission" includes any employee or contractor of the Commission, or employee of such contractor, to the extent that such employee or contractor of the Commission, or employee of such contractor prepares, disseminates, or provides access to, any information pursuant to his employment or contract with the Commission, or his employment with such contractor.